Trop J Nat Prod Res, May 2025; 9(5): 2167 - 2176 ISSN 2616-0684 (Print)
ISSN 2616-0692 (Electronic)

Tropical Journal of Natural Product Research

Available online at https://www.tjnpr.org

Original Research Article

In-Silico Molecular Docking and ADMET Prediction of Natural Compounds In *Oncom*

Irma R. Kartika[1]*, Azhar A. Syach[1], Diajeng Larasati[1], Shabrina A. Pitaloka[1], Sheila N. Octaviany[1], Fera Kurniadewi[1], Hanhan Dianhar[1], Irwan Saputra[1], Muktiningsih Nurjayadi[1], Rika S. Syaadah[2], Irah Namirah[3]

[1]*Chemistry Study Program, Faculty of Mathematics and Natural Sciences, Universitas Negeri Jakarta, Jalan Rawamangun Muka Jakarta 13220, Indonesia*
[2]*Chemistry Education Study Program, Faculty of Mathematics and Natural Sciences, Universitas Negeri Jakarta, Jalan Rawamangun Muka Jakarta 13220, Indonesia*
[3]*Chemistry Education Study Program, Faculty of Teacher Training and Education, Universitas Sultan Ageng Tirtayasa, Banten, 42117, Indonesia*

ARTICLE INFO

Article history:
Received 22 December 2024
Revised 10 April 2025
Accepted 12 April 2025
Published online 01 June 2025

ABSTRACT

Oncom is a traditional fermented cuisine from West Java, Indonesia, produced through the process of mold fermentation. *Oncom* is categorized into black *oncom* (BO) and red *oncom* (RO) based on the colour of the spore of the molds used in their fermentation. Both types of *oncom* are commonly found in traditional markets in West Java, Indonesia. This study aimed to explore and predict the diverse activities of bioactive compounds from both *oncom* by analyzing their interactions with multiple enzymes using the *in silico* method. The ethanol extracts of *oncom* were analyzed using liquid chromatography-high-resolution mass spectrometry (LC-HRMS). The absorption, distribution, metabolism, excretion, and toxicity (ADMET) predictions of the substances were performed using pkCSM and ProTox-II network servers, along with Lipinski's rule of five screening. Molecular docking was performed on *β*-lactamase (PDB ID: 1LLB), cytochrome P450 (PDB ID: 1JIP), human COX-2 (PDB ID: 3LN1), SARS-COV-2 protease (PDB ID: 6LU7), and protein kinase (PDB ID: 1MV5) using AutoDockTools. The LC-HRMS analysis revealed the presence of 64 compounds in *oncom* extracts. ADMET together with Lipinski's guidelines screening, predicted that nine of the 64 compounds showed promising biological activities. Daidzein exhibited a higher Gibbs free energy (ΔG) of -6.44 kcal/mol for 1LLB compared to clavulanic acid (-5.07 kcal/mol) and -5.91 kcal/mol for 1MV5 in contrast to verapamil (-4.04 kcal/mol). The findings indicate that daidzein exhibits potential inhibitory activity of bacterial infections and cancer cells.

Keywords: Absorption Distribution Metabolism Excretion Toxicity, Black *oncom*, Daidzein, Liquid Chromatography-High Resolution Mass Spectrometry, Red *oncom*

Introduction

Computer-Aided Drug Design (CADD) utilizes computational techniques tools, modeling techniques, and software to streamline and enhance the process of drug discovery and development.[1] CADD uses computational modeling to predict how potential drug candidates interact with biological targets, assess their effectiveness, and refine their properties, ultimately time-efficient, costs, biological and chemical databases for drug research.[2] Bioactive substances considered ideal as drug prospects are characterized by pharmacokinetics data (including absorption, distribution, metabolism, elimination, and comprehensive toxicological (ADMET) profiles).[3] According to Lipinski's pharmaceutical guidelines, oral bioavailability of drugs is affected by parameters such as dose, solvent affinity, and absorption capacity.[4] The specific goal of Rule of Five (Ro5) is to evaluate whether a compound can be efficiently absorbed through the gastrointestinal tract when taken orally.[5]

*Corresponding author. E mail: irmaratna@unj.ac.id
Tel: +62811937183

Citation: Kartika *et al*. *In-Silico* Molecular Docking and ADMET Prediction of Natural Compounds In *Oncom*. Trop J Nat Prod Res. 2025; 9(5): 2167 - 2176 https://doi.org/10.26538/tjnpr/v9i5.42

Official Journal of Natural Product Research Group, Faculty of Pharmacy, University of Benin, Benin City, Nigeria

Additionally, Lipinski's pharmaceutical rules offers an efficient approach to eliminate compounds with undesirable pharmacokinetic properties early in the drug development, optimizing time, and resources utilization.[6]

The binding site of the drug compound on the crystal structure data can be used to model the target protein available in Protein Data Bank (PDB).[7,8] Natural products are fundamental to pharmaceutical innovation. The biomolecules present in food and medical plants exhibit antioxidant, anti-inflammatory, and anticancer effects.[9] A quantitative structure-activity relationship study showed that these biomolecules can function as frameworks for molecular modification to improve the effectiveness, toxicological profile, and pharmacokinetics.[10]

Red *oncom* (RO) is derived from the byproducts of tofu production using *Neurospora* sp. (commonly called *N. sitophila*, *N.crassa* and/or *N. intermedia*), while black *oncom* (BO) is produced using *Rhizopus oligosporus* and *Mucor* sp. from peanut press cake, a byproduct of peanut oil extraction, with the addition of a little cassava flour (20% of the peanut cake weight)[11,12] The use of different molds and raw materials leads to the production of distinct compounds in each type of *oncom*. Previous studies revealed that the ethanol extract of RO contained daidzin, genistin, daidzein, and genistein at levels of 66.85, 132.56, 62.63, and 105.48 mg/100 g of dry basis (db), respectively.[13]

To the best of our understanding, no prior studies have been conducted on predicting biological activity using in silico methods and ADMET properties of *oncom*. Therefore, the objective of the research is to analyze the natural products profile of ethanol extract of black and red *oncom* sample using liquid chromatography-high-resolution mass spectrometry (LC-HRMS), a technique known for its high precision and accuracy in separating, identifying, and characterizing complex

compound mixtures. Furthermore, natural products were analyzed for ADMET properties using the pkCSM and ProTox-II web servers, alongside Lipinski's rule of five screening. Additionally, their potential inhibitory effects on *β*-lactamase, cytochrome P450, human COX-2, SARS-COV-2 protease, and protein kinase were investigated through *in-silico* approaches. The findings from the study could contribute to cancer prevention and therapy, and antibiotics development by targeting-multidrug-resistant organism.

Materials and Methods

Sample collection and extraction

The BO samples were collected in April 2024 from the traditional market of Pasar Ciparay Lama in Kabupaten Bandung, West Java, Indonesia (GPS of -7.0356227, 107.7135554). Meanwhile the RO samples were obtained in May 2024 from Pasar Kampung Ambon in East Jakarta, Indonesia (GPS of -6.1861568, 106.8843934). Both samples were air-dried and finally ground into powder. Approximately 500 mg of dried powder was extracted with 4 L of ethanol (purchased from Sigma Aldrich Co., Indofa, Surabaya, Indonesia) for five days at room temperature. The filtrate then was dried by rotary evaporation at 50°C. The extraction products were kept at 4°C until needed.

LC-HRMS analysis

LC-HRMS contained liquid chromatography (Thermo Scientific™ Vanquish™ UHPLC Binary Pump) couple with orbitrap high-resolution mass spectrometry (Thermo Scientific™ Q Exactive™ Hybrid Quadrupole-Orbitrap™). This instrumental analysis was employed to characterize the metabolites in each sample and was performed at the Laboratorium Biotek Rekayasa Indonesia in Bogor, Indonesia. The LC separation was performed using a ThermoScientific™ Accucore™ Phenyl-Hexyl column (100 mm × 2.1 mm ID × 2.6 μm), with a 3 μL injected sample. Two distinct solutions were utilized for the mobile phase. Solution A was 0.1% aqueous solution of formic acid, while Solution B comprised 0.1% methanolic solution of formic acid. The separation system followed a gradient profile: 0.00–0.01 min (5% B), 0.02–20.00 min (90% B), and 21.00–25.00 min (5% B), with a constant flow rate at 0.3 mL/min. The ionization source for UHPLC-Q-Orbitrap HRMS was ESI (positive/negative mode), using a Q-Orbitrap mass analyzer with an m/z detection range of 66.7–1000. Approximately 3.30 kV was applied for the spray voltage, with the capillary temperature of 320°C. The flow rates for the sheath gas, auxiliary gas, and sweep gas were 32, 8, and 4 AU, respectively. Resolution was 70,000 for full MS and 17,600 for dd-MS2.

ADMET prediction

ADMET prediction is the computational assessment of a compound's pharmacokinetics and safety profile.[14] It is a crucial early-stage drug discovery step to identify potential issues and optimize candidates before experimental testing.[8] The website https://biosig.lab.uq.edu.au/pkcsm/prediction was utilized to forecast the drug absorption and elimination of natural products. Furthermore, the ProTox-II website https://tox.charite.de/protox3/index.php?site=compound_input was used to predict the toxicological profile of the compounds. Toxicity classification is based on LD_{50} values: Class 1 (extremely lethal, ≤5 mg/kg), Class 2 (fatal, 5-50 mg/kg), Class 3 (toxic, 50-300 mg/kg), Class 4 (harmful, 300-2,000 mg/kg), Class 5 (possibly hazardous, 2,000-5,000 mg/kg), and Class 6 (nontoxic, >5,000 mg/kg).[15]

Lipinski's rule of five prediction

Physicochemical predictions of natural products were performed using the Lipinski's drug-likeness rules on the website http://www.scfbio-iitd.res.in/software/drugdesign/lipinski.jsp. The rule suggests that a drug-like molecule should adhere to the following criteria, allowing for at most one exception: its molecular weight should be under 500 daltons; the lipophilicity coefficient (LogP) should not exceed 5; the number of intermolecular hydrogen attraction donors needs to be 5 or less (combined OH and NH groups); and it should contain a maximum of 9 hydrogen bonding acceptor groups (total oxygen and nitrogen atoms).[16]

Equipment and software

The equipment used for data processing comprised a Hewlett-Packard laptop from 2018, equipped with an Intel(R) Core™ i5-8250U CPU @1.60GHz, 8 GB of RAM, and a Radeon 530 graphics card. It was pre-installed with the Windows 11 22H2 operating system. The software utilized included ChemDraw 18.1 (ChemOffice Suite 2018 by PerkinElmer) and Chem3D 18.1 (ChemOffice Suite 2018 by PerkinElmer), AutoDock4.2 Tools Version 1.5.7 (Molecular Graphics Lab (MGL) 2013 by The Scripps Research Institute), and BIOVIA Discovery Studio version 21.1.0.0, released by Dassault Systèmes in 2021.

Protein structure

The 3D crystal structure of proteins, including 1LLB, 1JIP, 3LN1, 6LU7, and 1MV5 were retrieved from the PDB database, with resolutions of 1.72, 2.00, 2.40, 2.16, and 3.10 Å, respectively. Their natural ligands (PCN, HEM, inhibitor N3, ATP) were also retrieved from PDB (http://www.rcsb.org).[17]

Natural products structure

The structures of selected natural products were downloaded from PubChem, ChemSpider, and DrugBank websites, and saved in sdf format. The positive controls, including celecoxib, clavulanic acid, ketoconazole, remdesivir, and verapamil were available for download in sdf format from DrugBank.

Preparation of protein and ligands (both native and test) for in silico study

Water molecules and natural ligands were eliminated from the enzyme complexes, then optimized in AutoDock4.2 by adding hydrogens atoms in polar bonds and electrostatic partial charges (Kollman charges). The resulting file was stored in pdbqt file type.[18] Meanwhile, the naturally derived substances that were consistently detected in *oncom* samples were prepared as test ligands by adding hydrogen atoms, assigning charges, and creating a torsion tree. The optimized ligands containing the PDB structure, partial charges (q), and atom types (t) were subsequently stored in pdbqt format.[19]

Docking simulation validation

Molecular docking validation was performed by creating grid boxes of different dimensions (40x40x40, 50x50x50, and 60x60x60).[20] Native ligands were used to test each grid size, and the optimal box size was determined based on the smallest inhibition constants (Ki) obtained from docking with the native ligands.[21]

Computational docking analysis of bioactive compounds

The confirmed grid box was applied for molecular docking, and the process was recorded in grid parameter file format. The following stage involved generating the dpf format (docking parameter data file) using the Lamarckian Genetic Algorithm (GA) method for executing AutoDock4.2. Notepad application was used to view the docking parameters (such as values of binding affinity (ΔG), Ki, and root mean square deviation (RMSD)) in the dlg data file. The binding poses of each ligand and the BIOVIA Discovery Studio 21.1.0.0 was employed to visualize the interaction between ligands and enzymes.[22]

Results and Discussion

Extraction yield and LC-HRMS analysis

Ethanol was selected as the solvent for the extraction of the phytochemical compounds present in *oncom* samples. The extraction yields of BO and RO were 10% and 7%, respectively. LC-HRMS analysis identified 64 compounds in all extracts, including lipids, vitamin B, amino acids, isoflavones, alkaloids, and aromatic amines (Table 1). Moreover, based on ADMET prediction and the rule of five for drug-likeness, nine bioactive compounds were successfully identified as detailed in Table 2.

Table 1: Compounds in RO and BO based on LC-HRMS analysis

No.	Name of Compound (Pub Chem CID)	Molecular Formula	Molecular Weight (g/mol)	Percentage (%)	
				RO	BO
1	2,3-Dihydroxypropyl (9Z,12Z)-octadeca-9,12-dienoate (5283469)	$C_{21}H_{38}O_4$	354.276	2.256	2.809
2	(10E,12E)-9-Oxooctadeca-10,12-dienoic acid (5283011)	$C_{18}H_{30}O_3$	294.218	0.208	2.726
3	(2R)-Piperidine-2-carboxylic acid (736316)	$C_6H_{11}NO_2$	129.079	0.100	0.333
4	2,3-Dihydroxypropyl (Z)-octadec-9-enoate (5283468)	$C_{21}H_{40}O_4$	356.292	0.912	1.530
5	Ethyl tetradecanoate (31283)	$C_{16}H_{32}O_2$	256.240	0.249	0.010
6	Ethyl (Z)-octadec-9-enoate (5363269)	$C_{20}H_{38}O_2$	310.286	1.549	2.813
7	(9Z,12Z)-N-(2-Hydroxyethyl)octadeca-9,12-dienamide (5283446)	$C_{20}H_{37}NO_2$	323.281	0.026	0.160
8	Methyl hexadecanoate (8181)	$C_{17}H_{34}O_2$	270.255	0.032	0.016
9	Octadecanoic acid (5281)	$C_{18}H_{36}O_2$	284.271	1.786	0.781
10	(2R)-Pyrrolidine-2-carboxylic acid (8988)	$C_5H_9NO_2$	115.063	0.070	0.348
11	D-(+)-Pyroglutamic acid (439685)	$C_5H_7NO_3$	129.043	0.225	0.073
12	(2S)-2-Amino-5-(diaminomethylideneamino)pentanoic acid (6322)	$C_6H_{14}N_4O_2$	174.111	0.112	0.054
13	(2S)-2-Aminopentanedioic acid (33032)	$C_5H_9NO_4$	147.053	0.387	0.663
14	N-(4-Ethoxyphenyl)acetamide (4754)	$C_{10}H_{13}NO_2$	179.094	0.072	0.138
15	2-Methyl-1,2-dipyridin-3-ylpropan-1-one (4174)	$C_{14}H_{14}N_2O$	226.110	0.144	0.200
16	(1S,9S,10S)-4-Methoxy-17-methyl-17-azatetracyclo[7.5.3.01,10.02,7]heptadeca-2(7),3,5-triene (5360696)	$C_{18}H_{25}NO$	271.193	0.295	0.037
17	7-Hydroxy-3-(4-hydroxyphenyl)chromen-4-one (5281708)	$C_{15}H_{10}O_4$	254.057	0.849	0.247
18	5,7-Dihydroxy-3-(4-hydroxyphenyl)chromen-4-one (5280961)	$C_{15}H_{10}O_5$	270.052	0.395	0.146
19	7-Hydroxy-3-(4-hydroxyphenyl)-6-methoxychromen-4-one (5317750)	$C_{16}H_{12}O_5$	284.068	0.041	0.023
20	Pyridine-3-carboxylic acid (938)	$C_6H_5NO_2$	123.032	0.907	0.198
21	4-(4-Amino-3-methylphenyl)-2-methylaniline (8413)	$C_{14}H_{16}N_2$	212.131	0.167	0.003
22	N-phenylacetamide (904)	C_8H_9NO	135.068	0.306	0.147
23	8-[(1S,5S)-4-Oxo-5-[(Z)-pent-2-enyl]cyclopent-2-en-1-yl]octanoic acid (5280411)	$C_{18}H_{28}O_3$	292.204	0.000	0.062
24	2,3,4,9-Tetrahydro-1H-pyrido[3,4-b]indole-3-carboxylic acid (98285)	$C_{12}H_{12}N_2O_2$	216.090	0.000	0.039
25	2-Aminooctadecane-1,3,4-triol (248575)	$C_{18}H_{39}NO_3$	317.292	0.000	0.590
26	3-Hydroxypyridine-2-carboxylic acid (13401)	$C_6H_5NO_3$	139.027	0.000	0.041
27	1-Phenylethanone (7410)	C_8H_8O	120.057	0.000	0.595
28	Methyl 1-methyl-3,6-dihydro-2H-pyridine-5-carboxylate (2230)	$C_8H_{13}NO_2$	155.095	0.000	0.031
29	4-(4-Aminophenyl)aniline (7111)	$C_{12}H_{12}N_2$	184.100	0.000	0.063
30	(3S)-3-Hydroxy-4-(trimethylazaniumyl)butanoate (2724480)	$C_7H_{15}NO_3$	161.105	0.000	0.079
31	2,6-Diaminohexanoic acid (866)	$C_6H_{14}N_2O_2$	146.105	0.000	0.027
32	Docosanamide (76468)	$C_{22}H_{45}NO$	339.349	0.000	0,050
33	Hexadecanamide (69421)	$C_{16}H_{33}NO$	255.256	0.000	0.035
34	1H-Indole (798)	C_8H_7N	117.058	0.000	0.076
35	(2S)-1-[(2S)-2-Aminopropanoyl]pyrrolidine-2-carboxylic acid (83525)	$C_8H_{14}N_2O_3$	186.100	0.000	0.049
36	(2S)-2-Amino-3-(4-hydroxyphenyl)propanoic acid (6057)	$C_9H_{11}NO_3$	181.074	0.000	0.026
37	N-[2-(1H-Imidazol-5-yl)ethyl]acetamide (69602)	$C_7H_{11}N_3O$	153.090	0.000	0.043
38	(Z)-N-(2-Hydroxyethyl)octadec-9-enamide (5283454)	$C_{20}H_{39}NO_2$	325.297	0.000	0.104
39	1-(Propan-2-ylamino)-3-(2-prop-2-enoxyphenoxy)propan-2-ol (4631)	$C_{15}H_{23}NO_3$	265.168	0.000	0.013
40	N-(2-Hydroxyethyl)hexadecanamide (4671)	$C_{18}H_{37}NO_2$	299.282	0.000	0.031
41	(2S)-1-(Tert-butylamino)-3-(2-cyclopentylphenoxy)propan-2-ol (37464)	$C_{18}H_{29}NO_2$	291.220	0.000	0.014
42	1-(1-Phenylpentan-2-yl)pyrrolidine (14592)	$C_{15}H_{23}N$	217.183	0.000	0.026

43	1-Naphthalen-1-yloxy-3-(propan-2-ylamino)propan-2-ol (4946)	$C_{16}H_{21}NO_2$	259.157	0.000	0.041
44	Butane-1,4-diamine (1045)	$C_4H_{12}N_2$	88.100	0.000	0.012
45	2-Phenyl-2-piperidin-2-ylacetic acid (86863)	$C_{13}H_{17}NO_2$	219.126	0.000	0.102
46	5-methyl-1H-pyrimidine-2,4-dione (1135)	$C_5\ H_6N_2O_2$	126.043	0.000	0.062
47	N-Ethyl-3-hydroxy-2-phenyl-N-(pyridin-4-ylmethyl)propanamide (5593)	$C_{17}H_{20}N_2O_2$	284.153	0.000	0.018
48	1H-Pyrimidine-2,4-dione (1174)	$C_4H_4N_2O_2$	112.027	0.000	0.259
49	(2S)-1-[(2S)-2-Amino-3-methylbutanoyl]pyrrolidine-2-carboxylic acid (9837272)	$C_{10}H_{18}N_2O_3$	214.132	0.000	0.065
50	4-Aminobutanoic acid (119)	$C_4H_9NO_2$	103.064	0.000	0.073
51	1,2,3-Trihydroxyhenicosan-4-one (22035687)	$C_{21}H_{42}O_4$	358.307	0.594	0.000
52	4-(Diaminomethylideneamino)butanoic acid (500)	$C_5H_{11}N_3O_2$	145.085	0.074	0.000
53	(3R)-3-Acetyloxy-4-(trimethylazaniumyl)butanoate (7045767)	$C_9H_{17}NO_4$	203.115	0.438	0.000
54	(2R,3R,4S,5R)-2-(6-Aminopurin-9-yl)-5-(hydroxymethyl)oxolane-3,4-diol (60961)	$C_{10}H_{13}N_5O_4$	267.097	0.171	0.000
55	Ethyl (Z)-hexadec-9-enoate (6436624)	$C_{18}H_{34}O_2$	282.255	0.047	0.000
56	3-Hydroxy-4-(trimethylazaniumyl)butanoate (288)	$C_7H_{15}NO_3$	161.105	0.233	0.000
57	Ethyl dodecanoate (7800)	$C_{14}H_{28}O_2$	228.208	0.150	0.000
58	(2S)-2-Amino-3-phenylpropanoic acid (6140)	$C_9H_{11}NO_2$	165.079	0.190	0.000
59	2,3-Dihydroxypropyl dodecanoate (14871)	$C_{15}H_{30}O_4$	274.214	0.112	0.000
60	(2R)-2-[(3R,4R,5S,6R)-3-Amino-2,5-dihydroxy-6-(hydroxymethyl)oxan-4-yl]oxypropanoic acid (441038)	$C_9H_{17}NO_7$	251.100	0.032	0.000
61	(3R,5S)-3-Hydroxy-1-methyl-5-pyridin-3-ylpyrrolidin-2-one (107963)	$C_{10}H_{12}N_2O_2$	192.090	0.119	0.000
62	8-Methyl-8-azabicyclo[3.2.1]octan-3-one (79038)	$C_8H_{13}NO$	139.099	0.580	0.000
63	(2S)-2-Amino-3-methylbutanoic acid (6287)	$C_5H_{11}NO_2$	117.079	0.343	0.000
64	(9Z,12Z,15Z)-Octadeca-9,12,15-trienoic acid (5280934)	$C_{18}H_{30}O_2$	278.224	0.399	0.000

Table 2: Bioactive compounds based on ADMET prediction and Lipinski's rule of five

No	Name of Compound (Pub Chem CID)	Molecular Formula	Molecular Weight (g/mol)	Structure
17	7-Hydroxy-3-(4-hydroxyphenyl)chromen-4-one (5281708)	$C_{15}H_{10}O_4$	254.057	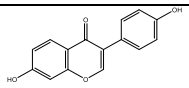
18	5,7-Dihydroxy-3-(4-hydroxyphenyl)chromen-4-one (5280961)	$C_{15}H_{10}O_5$	270.052	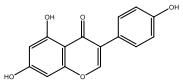
20	Pyridine-3-carboxylic acid (938)	$C_6H_5NO_2$	123.032	
24	2,3,4,9-Tetrahydro-1H-pyrido[3,4-b]indole-3-carboxylic acid (98285)	$C_{12}H_{12}N_2O_2$	216.090	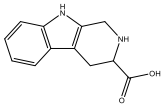
26	3-Hydroxypyridine-2-carboxylic acid (13401)	$C_6H_5NO_3$	139.027	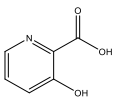
36	(2S)-2-Amino-3-(4-hydroxyphenyl)propanoic acid (6057)	$C_9H_{11}NO_3$	181.074	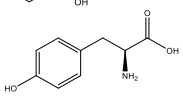
37	N-[2-(1H-Imidazol-5-yl)ethyl]acetamide (69602)	$C_7\ H_{11}N_3O$	153.090	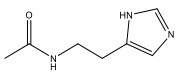

39	1-(Propan-2-ylamino)-3-(2-prop-2-enoxyphenoxy)propan-2-ol (4631)	$C_{15}H_{23}NO_3$	265.168	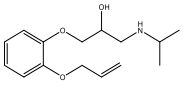
63	(2S)-2-Amino-3-methylbutanoic acid (6287)	$C_5H_{11}NO_2$	117.079	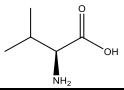

ADMET prediction

Table 3 summarizes the ADMET properties of the nine compounds based on computational analysis, while Table 4 presents their toxicity class predictions. The pharmacokinetic data in Table 2 indicates that none of the bioactive compounds inhibit CYP3A4 enzymes, ensuring their compatibility with various CYP3A4 substrates. This is significant as CYP3A4 metabolizes more than 50% of drugs processed by CYP enzymes and approximately 46% of the 200 most frequently used prescription drugs in the United States.[23]

Table 3: The ADMET properties of the nine selected compounds

Properties	17	18	20	24	26	36	37	39	63	**Unit**
Absorption										
Water solubility	-3.793	-3.595	2.134	-2.367	-2.421	-2.89	-2.017	-2.089	-2.888	Numeric (log mol/L)
Caco2 permeability	0.903	0.9	1.17	0.619	0.567	0.553	1.111	1.451	0.541	Numeric (log Papp in 10^{-6} cm/s)
Intestinal absorption (human)	94.839	93.387	94.099	79.974	92.178	73.014	71.976	91.85	76.187	Numeric (% Absorbed)
Skin Permeability	-2.748	-2.735	-2.735	-2.735	-2.735	-2.735	-2.735	-2.953	-2.736	Numeric (log Kp)
P-glycoprotein substrate	Yes	Yes	No	Yes	No	Yes	Yes	No	No	Categorical (Yes/No)
P-glycoprotein I inhibitor	No	No	No	No	No	No	No	No	No	Categorical (Yes/No)
P-glycoprotein II inhibitor	No	No	No	No	No	No	No	No	No	Categorical (Yes/No)
Distribution										
VDss (human)	-0.172	0.094	-1.015	-1.325	-0.537	-0.225	-0.504	0.872	-0.572	Numeric (log L/kg)
Fraction unbound (human)	0.107	0.087	0.776	0.432	0.826	0.535	0.685	0.403	0.462	Numeric (Fu)
BBB permeability	-0.064	-0.71	-0.323	-0.292	0.151	-0.698	-0.346	-0.163	-0.354	Numeric (log BB)
CNS permeability	-1.992	-2.048	-2.869	-2.401	-3.314	-2.843	-3.451	-2.901	-3.353	Numeric (log PS)
Metabolism										
CYP2D6 substrate	No	No	No	Yes	No	No	No	No	No	Categorical (Yes/No)
CYP3A4 substrate	No	No	No	No	No	No	No	No	No	Categorical (Yes/No)
CYP1A2 inhibitior	Yes	Yes	No	No	No	No	No	Yes	No	Categorical (Yes/No)
CYP2C19 inhibitior	Yes	Yes	No	No	No	No	No	No	No	Categorical (Yes/No)
CYP2C9 inhibitior	Yes	No	No	No	No	No	No	No	No	Categorical (Yes/No)
CYP2D6 inhibitior	No	No	No	No	No	No	No	Yes	No	Categorical (Yes/No)
CYP3A4 inhibitior	No	No	No	No	No	No	No	No	No	Categorical (Yes/No)
Excretion										
Total Clearance	0.164	0.151	0.652	0.786	0.672	0.436	1.107	0.768	0.205	Numeric (log ml/min/kg)
Renal OCT2 substrate	No	No	No	No	No	No	No	No	No	Categorical (Yes/No)
Toxicity										
AMES toxicity	No	No	No	No	No	No	No	No	No	Categorical (Yes/No)
Max, tolerated dose (human)	0.187	0.478	0.907	0.837	0.772	0.963	-0.584	0.996	1.137	Numeric (log mg/kg/day)
hERG I inhibitor	No	No	No	No	No	No	No	No	No	Categorical (Yes/No)
hERG II inhibitor	No	No	No	No	No	No	No	No	No	Categorical (Yes/No)
Oral Rat Acute Toxicity	2.164	2.268	2.24	2.31	2.119	2.197	2.491	2.497	2.019	Numeric (mol/kg)
Oral Rat Chronic Toxicity	1.187	2.189	2.652	1.172	2.677	2.036	1.191	1.666	2.901	Numeric (log mg/kg_bw/day)
Hepatotoxicity	No	No	No	No	No	No	No	No	No	Categorical (Yes/No)

Skin Sensitisation	No	No	No	No	No	No	No	No	No	Categorical (Yes/No)
T,Pyriformis toxicity	0.693	0.377	0.055	0.285	0.281	0.275	0.285	1.026	0.184	Numeric (log ug/L)
Minnow toxicity	1.035	1.941	2.222	1.216	1.847	2.504	2.795	2.212	2.422	Numeric (log mM)

Table 4: The toxicity prediction of nine compounds

Parameters	**17**	**18**	**20**	**24**	**26**	**36**	**37**	**39**	**63**
Predicted LD_{50} (mg/kg)	2,430	2,500	3,720	300	600	1,460	1,000	214	12,680
Predicted toxicity class	Class 5	Class 5	Class 5	Class 3	Class 4	Class 4	Class 4	Class 3	Class 6
Average similarity	97.3%	87.09%	100.00%	58.29%	64.61%	88.35%	63.62%	100.00%	75.00%
Prediction accuracy	72.9%	70.97%	100.00%	67.38%	68.07%	70.97%	68.07%	100.00%	69.26%

Toxicity, another pharmacokinetic predictor, reveals that the nine compounds are non-mutagenic, non-skin-sensitizing, non-hepatic toxic, and do not blocking hERG I or hERG II, which are encoded by the hERG gene and contribute to heart rate regulation. Furthermore, the nine compounds were considered favorable and exhibited low maximum tolerated dose based on both acute oral toxicity in rats (LD_{50}) and chronic oral toxicity in rats (LOAEL) doses. Table 4 shows that compound 63 is classified as nontoxic (Class 6, $LD_{50} > 5{,}000$), compounds 17, 18, and 20 as possibly hazardous (Class 5, $2{,}000 < LD_{50} \leq 5{,}000$), compounds 26, 36, and 37 as harmful (Class 4, $300 < LD_{50} \leq 2{,}000$), and compounds 24 and 39 as toxic (Class 3, $50 < LD_{50} \leq 300$). The LD_{50} value, an indicator of acute toxicity, represents the amount of substances necessary to lethally affect 50% of test population, with lower LD_{50} values indicating higher toxicity.[15]

Predictions of Lipinski's rule of five

Table 5 displays the oral bioavailability rules predictions for the nine compounds. All compounds complied with the Lipinski's rules, meaning that these compounds are likely to be efficiently absorbed through oral administration. As shown in Table 5, compound 17 demonstrated better absorption and higher permeability compared to the other compounds.[16]

Table 5: The prediction of Lipinski's Rule of Five for the nine compounds

Parameters	**17**	**18**	**20**	**24**	**26**	**36**	**37**	**39**	**63**
MW < 500 daltons	254.057	270.052	123.032	216.090	139.027	181.074	153.090	265.168	117.079
Hydrogen bond donors < 5	2	3	1	3	2	4	2	2	3
HBA < 10	4	5	3	3	4	4	3	4	3
Lipophilicity (LogP < 5)	2.408	2.114	0.780	1.034	0.485	0.347	0.088	1.989	0.054
Molar Refractivity (40-130)	69.344	71.001	31.196*	59.333	32.861*	47.422	40.975	76.774	30.449*

Molecular docking validation

The initial step focused on validating the docking of each native ligand into the active sites of five proteins, using grid box dimensions of 40, 50, and 60. The grid box with the lowest binding energy (ΔG) and inhibition constant (Ki) was chosen for molecular docking to conform that the bioactive compounds accurately bind to the five proteins, producing the desired pharmacological effect.[24] Grid box validation for the five proteins was conducted at dimensions of 40 or 50, as indicated in Table 6.

Table 6: The outcomes of the model validation analysis

Protein	**Native Ligand www.rcsb.org**	**Grid Size (points)**	**Coordinates of the Grid Center**	**Energy Gibbs (kcal/mol)**			
				1	**2**	**3**	**Mean**
1LLB	2-{1-[2-(2-Amino-thiazol-4-yl)-2-methoxyimino-acetylamino]-2-oxo-ethyl}-5,5-dimethyl-thiazolidine-4-carboxylic acid, $C_{14}H_{19}N_5O_5S_2$ (PCN)	40x40x40		-4.14	-3.65	-3.16	-3.65
		50x50x50	x: 80.945 y: 5.596 z: 30.484	-3.03	-3.57	-4.08	-3.56
		60x60x60		-4.15	-3.17	-2.71	-3.34
1JIP	Protoporphyrin IX Containing Fe $C_{34}H_{32}FeN_4O_4$ (HEM)	40x40x40	x: -9.673	-15.05	-14.92	-15.04	-15.00
		50x50x50	y: 13.396	-15.07	-15.07	-15.00	-15.05
		60x60x60	z: 10.738	-14.99	-14.94	-14.92	-14.95
3LN1	Protoporphyrin IX containing Fe, $C_{34}H_{32}FeN_4O_4$ (HEM)	40x40x40	x: 30.476	-14.16	-14.13	-14.19	-14.16
		50x50x50	y: -36.735	-14.16	-14.24	-14.25	-14.22
		60x60x60	z: -2.473	-14.03	-14.15	-14.20	-14.13

6LU7	N-[(5-methylisoxazol-3-yl)carbonyl]alanyl-l-valyl-N~1~-((1R,2Z)-4-(benzyloxy)-4-oxo-1-{[(3R)-2-oxopyrrolidin-3-yl]methyl}but-2-enyl)-l-leucinamide (inhibitor N3)	40x40x40		-5.37	-5.95	-5.62	-5.65
		50x50x50	x: -11.751 y: 14.39 z: 65.199	-5.48	-5.38	-5.46	-5.44
		60x60x60		-5.35	-5.60	-5.36	-5.44
1MV5	Adenosine-5'-triphosphate $C_{10}H_{16}N_5O_{13}P_3$ (ATP)	40x40x40	x: 35.834	-6.82	-6.87	-6.40	-6.70
		50x50x50	y: 34.721	-5.62	-6.64	-5.90	-6.05
		60x60x60	z: 76.35	-6.03	-5.30	-6.55	-5.96

In this study, five activities were evaluated: antibacterial activity through a *β*-lactamase inhibition pathway (1LLB), inhibiting cytochrome P450 51 (CYP51) induces antifungal activity (1JIP), blocking COX-2 as anti-inflammatory action (3LN1), antiviral potential via inhibition of the catalytic pocket of SARS-CoV-2 Mpro (6LU7), and P-GP inhibition against cancer (1MV5). The most promising molecule was identified by screening nine model compounds on the above five selected enzymes. Table 7 presents the predicted Gibbs free energy (ΔG) and inhibition constants (Ki) values of nine compounds obtained from the molecular docking analysis. Daidzein (17 or 7-hydroxy-3-(4-hydroxyphenyl)chromen-4-one) displayed the highest Gibbs free energy for the five proteins (3LN1, 1LLB, 1JIP, 6LU7, 1MV5).

Table 7: The docking results of nine compounds with five proteins

Protein	Docking parameter	Compound 17	18	20	24	26	36	37	39	63
1LLB	**ΔG (Kcal/mol)**	-6.44	-6.39	-4.50	-5.71	-4.08	-4.57	-4.01	-4.29	-3.20
	Ki (μM)	19.13	20.61	498.87	65.16	1,020	450.59	1,160	715.27	4,530
1JIP	**ΔG (Kcal/mol)**	-6.71	-5.96	-4.25	-6.13	-3.85	-4.53	-4.34	-4.35	-3.63
	Ki (μM)	12.12	43.02	770.88	32.26	1,510	474.33	662.89	646.01	2,180
3LN1	**ΔG (Kcal/mol)**	-7.68	-7.54	-4.52	-6.92	-4.59	-5.51	-4.94	-6.31	-3.51
	Ki (μM)	2.37	2.98	484.02	8.47	431.27	90.94	239.23	23.75	2,680
6LU7	**ΔG (Kcal/mol)**	-6.60	-6.32	-3.65	-5.99	-4.20	-4.72	-4.25	-5.72	-3.43
	Ki (μM)	14.43	23.38	2,100	40.96	831.17	345.97	767.07	64.48	3,050
1MV5	**ΔG (Kcal/mol)**	-5.91	-5.13	-4.32	-5.46	-4.77	-4.30	-4.11	-4.45	-3.58
	Ki (μM)	46.29	174.36	680.15	98.97	319.25	704.37	704.37	548.76	2,360

The predicted binding energy (ΔG) values of daidzein with the five proteins are illustrated in Table 8. Docking analysis for antibacterial activity was conducted by targeting *β*-lactamase inhibition using PDB codes 1LLB (*E. coli* AmpC *β*-lactamase in complex with ATMO-penicillin). The binding of nine compounds with the 1LLB receptors were evaluated against clavulanic acid as the reference. Daidzein displayed a higher ΔG values (-6.44 kcal/mol) for 1LLB than clavulanic acid (-5.07 kcal/mol), indicating its potential antibacterial activity and efficacy in countering *β*-lactamase-mediated multidrug resistance through *β*-lactamase inhibition.[25] Previous report demonstrated that the synergistic interaction with daidzein (400 μg/mL) lowered the average gentamicin minimum inhibitory concentration (MIC) against *A. baumannii* from 27 to 8 μg/mL, which may help mitigate antibiotic resistance.[26] Moreover, daidzein effectively disrupted *E. coli* DNA gyrase activity, yielding an IC_{50} of 0.042 μg/mL, in contrast to ciprofloxacin (IC_{50} = 0.018 μg/mL).[27] Furthermore, as illustrated in Figure 1, daidzein binding to 1LLB forms three hydrogen bonds with ALA318, ASN152, and ASN346.

Table 8: The predicted binding energy (ΔG) values of compound 17 with five proteins

Activities	Mechanism of action	PDB-ID	Positive control		17
Antibacterial	Beta-lactamase inhibitor	1LLB	Clavulanic acid	-5.07	-6.44
Antifungal	CYP450-dependent 14-alpha demethylase inhibitor	1JIP	Ketoconazole	-8.63	-6.71
Anti-inflammatory	COX-2 inhibitor	3LN1	Celecoxib	-8.21	-7.68
Antiviral	3CL-pro inhibitor	6LU7	Remdesivir	-6.80	-6.60
Anticancer	P-GP inhibitor	1MV5	Verapamil	-4.04	-5.91

ISSN 2616-0684 (Print)
ISSN 2616-0692 (Electronic)

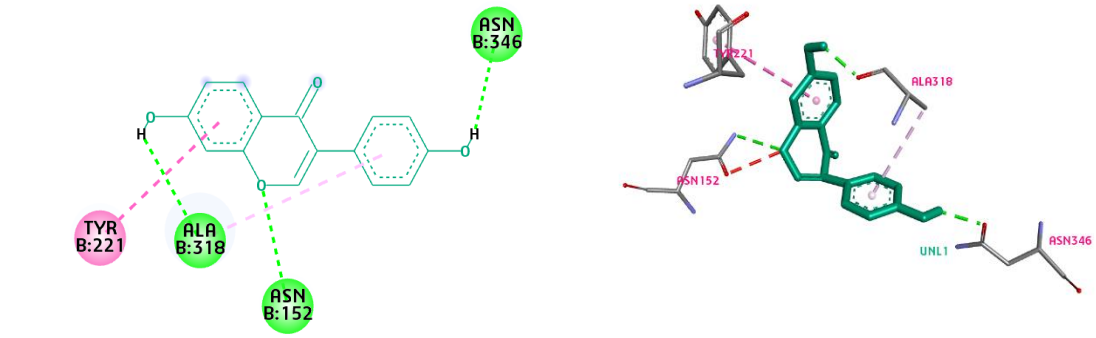

Daidzein-1LLB

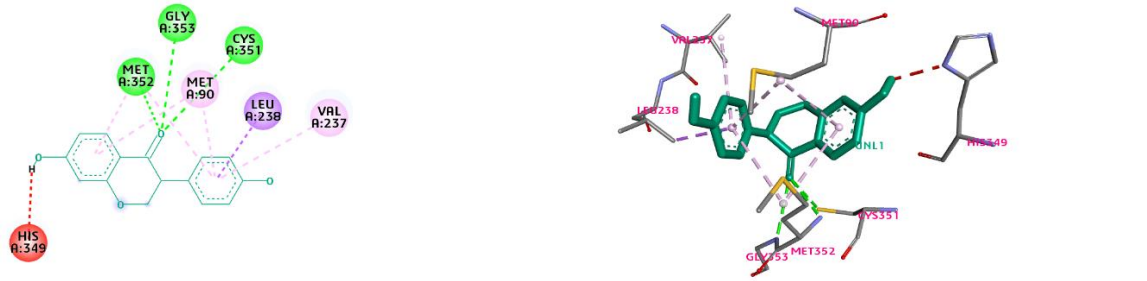

Daidzein-1JIP

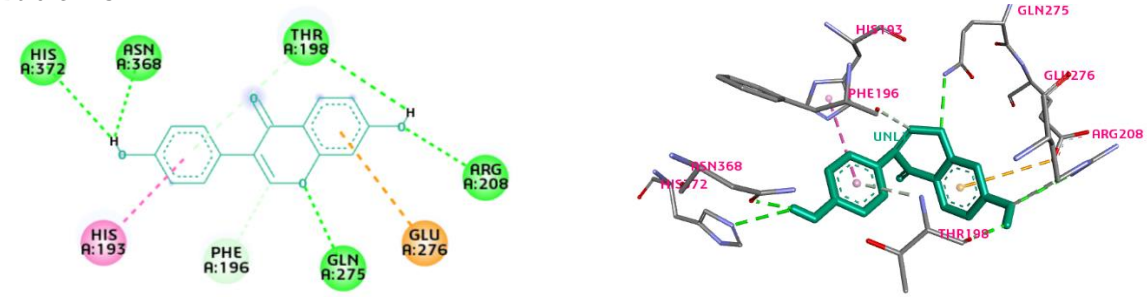

Daidzein-3LN1

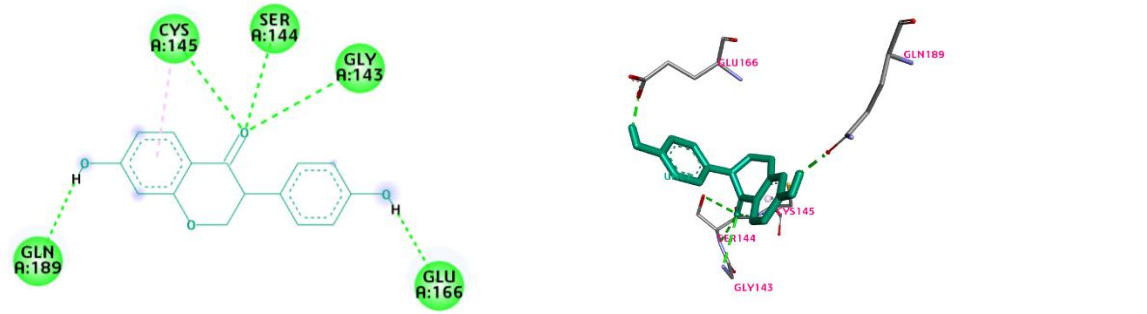

Daidzein-6LU7

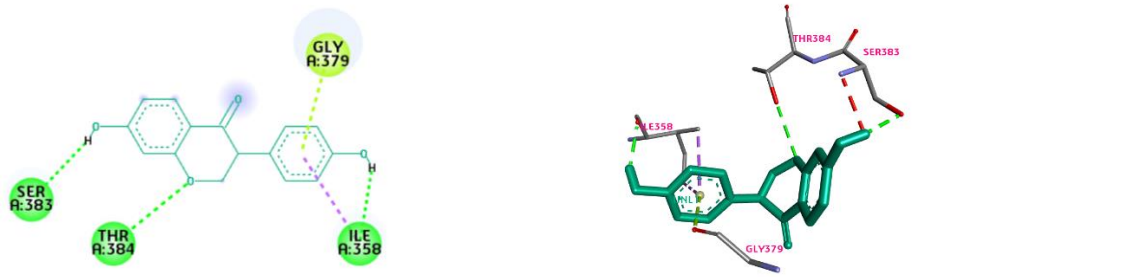

Daidzein-1MV5

Figure 1: 2D and 3D daidzein-target interactions at binding site of 1LLB, 1JIP, 3LN1, 6LU7, and 1MV5

Docking simulation for antifungal activity was performed via binding to CYP51 enzyme (1JIP), using ketoconazole-induced modifications in the binding site of cytochrome P450 proteins in mammals as the mechanism of inhibition. At this stage, the interactions between the nine compounds and 1JIP receptor were examined against ketoconazole as the reference. Daidzein displayed a ΔG value of -6.71 kcal/mol, which was higher than those of the other compounds, but lower than the ΔG value of ketoconazole (-8.63 kcal/mol). These results suggest that daidzein may not demonstrate antifungal activity via CYP450 inhibition. Additional research exploring other mechanisms of antifungal activity for daidzein is required.

Computational docking was carried out to assess anti-inflammatory response via COX-2 inhibition (3LN1), with celecoxib interacting with the COX-2 enzyme active site. Daidzein showed a ΔG value of -7.68 kcal/mol, higher than other compounds but lower than that of celecoxib (-8.21 kcal/mol). These findings suggest that daidzein may not exhibit anti-inflammatory activity via COX-2 enzyme suppression, and further research into its activity through other modes of action is needed.

Ligand-receptor interaction was conducted to assess viral inhibition through 3CL-pro enzyme inhibition (PDB code 6LU7), using remdesivir as the standard for comparison. Daidzein showed a ΔG value of -6.60 kcal/mol, higher than other compounds but lower than that of remdesivir (-6.80 kcal/mol). These findings suggest that daidzein may not exhibit antiviral potential against SARS-CoV-2 mediated by 3CL-pro inhibition. Further investigation into its antiviral activity through different mechanisms is essential.

Molecular interaction modeling was conducted to assess anticancer activity through P-GP inhibition using 1MV5 (LmrA ATP-binding domain). The interactions of nine compounds with these receptors were measured against verapamil as the reference compound. Daidzein exhibited a higher ΔG value (-5.91 kcal/mol) than verapamil (-4.40 kcal/mol), suggesting that daidzein may counter P-GP-mediated multidrug resistance and potentially display anticancer activity via P-GP inhibition. Additionally, previous studies have shown that daidzein inhibited A-375 melanoma cell proliferation, mediated G0/G1 phase arrest (by downregulating cyclin D1, CDK4, CDK6, and p27 expression), triggered apoptosis (through Bcl-2 depletion, Bax increase, caspase-3/-9 activation, and triggers cytochrome C release), promoted autophagy (by increasing LC3B II and decreasing p62).[28] Daidzein promoted mitochondrial-regulated apoptosis in MCF-7 breast cancer cells (IC_{50} = 50 μM) by increasing ROS levels, caspase 3/7 activity, and annexin V staining while also downregulating ERα and upregulating ERβ, further enhancing apoptosis and inhibiting cell proliferation.[29] TNF-α, IL-6, and IL-1β act as pro-inflammatory signaling molecules that drive cancer progression by promoting inflammation, proliferation, survival, angiogenesis, and metastasis, while daidzein counteracted these effects by inhibiting LPS-induced inflammation in macrophages, reducing NO and PGE2 production, and suppressing the canonical inflammasome pathway, which lead to decreased NLRP3 regulation and reduced IL-1β and IL-18 activation.[30] Daidzein alleviated OVX-induced osteoporosis by promoting H-type vessel generation in trabecular bone, enhancing new bone synthesis through upregulation of EGFR/PI3K/AKT signaling, primarily by inhibiting Cav-1 in endothelial cells.[31] Furthermore, as shown in Figure 1, daidzein binding to 1MV5 establishes three hydrogen bonds with ILE358, SER383, and THR384.

Conclusion

The study suggested that daidzein had higher Gibbs energy (ΔG) than clavulanic acid and verapamil. These findings imply that daidzein has promise as inhibitors of bacterial infections and cancer cells. Future studies will investigate the impact of daidzein on cellular signalling pathways in living organisms, emphasizing its role in inflammation, oxidative stress, and cell survival. These findings could have valuable applications in cancer prevention and antibiotic development by targeting multidrug resistance mechanisms**.**

Conflict of Interest

The authors declare no conflicts of interest.

Authors' Declaration

The authors hereby declare that the works presented in this article are original and that any liability for claims relating to the content of this article will be borne by them.

Acknowledgement

The authors gratefully acknowledge the Direktorat Riset, Teknologi dan Pengabdian kepada Masyarakat, Ministry of Education, Culture, Research and Technology of the Republic of Indonesia for their support through the Penelitian Fundamental Reguler (PFR) funding (Grant Number: 5/UN39.14/PG.02.00.PL/PFR/VI/2024). We would also like to thank Osayemwenre Erharuyi for editing and proofreading this manuscript in English.

References

1. Niazi SK and Mariam Z. Computer-Aided Drug Design and Drug Discovery: A prospective Analysis. Pharmaceuticals. 2024; 17(1):1-22. doi: 10.3390/ph17010022
2. Dhudum R, Ganeshpurkar A, Pawar A. Revolutionizing Drug Discovery: A Comprehensive Review of AI Applications. Drug Drug Candidates. 2024; 3(1):148-171. doi: 10.3390/ddc3010009
3. Stielow M, Witczyńska A, Kubryń N, Fijałkowski Ł, Nowaczyk J, Nowaczyk A. The Bioavailability of Drugs—The Current State of Knowledge. Molecules. 2023; 28(8038):1-19. doi: 10.3390/molecules28248038
4. Rai M, Singh AV, Paudel N, Kanase A, Falletta E, Kerkar P, Heyda J, Barghash RF, Singh SP, Soos M. Herbal Concoction Unveiled: A Computational Analysis of Phytochemicals' Pharmacokinetic and Toxicological Profiles Using Novel Approach Methodologies (NAMs). Curr Res Toxicol. 2023; 5100118):1-13. doi: 10.1016/j.crtox.2023.100118
5. Nhlapho S, Nyathi MHL, Ngwenya BL, Dube T, Telukdarie A, Munien I, Vermeulen A, Chude-Okonkwo UAK. Druggability of Pharmaceutical Compounds Using Lipinski Rules with Machine Learning. Pharm. Sci. 2024; 3(4):177-192. doi: 10.58920/sciphar0304264
6. Bitew M, Desalegn T, Demissie TB, Belayneh A, Endale M, Eswaramoorthy R. Pharmacokinetics and Drug-likeness of Antidiabetic Flavonoids: Molecular Docking and DFT Study. PLoS One. 2021; 16(12):1-22. doi: 10.1371/journal.pone.0260853
7. Goodsell DS, Zardecki C, Di Costanzo L, Duarte JM, Hudson BP, Persikova I, Segura J, Shao C, Voight M, Westbrook JD, Young JY, Burley SK. RCSB Protein Data Bank: Enabling Biomedical Research and Drug Discovery. Protein Sci. 2020; 29(1):52-65. doi: 10.1002/pro.3730
8. Singh N, Vayer P, Tanwar S, Poyet J-L, Tsaioun K, Villoutreix BO. Drug Discovery and Development: Introduction to the General Public and Patient Groups. Front Drug Discov. 2023; 3:1-11. doi: 10.3389/fddsv.2023.1201419
9. Wardana AP, Aminah NS, Kristanti AN, Fahmi MZ, Abdjan MI, Sucipto TH. Antioxidant, Anti-inflammatory, Antiviral and Anticancer Potentials of *Zingiberaceae* Species Used as Herbal Medicine in Indonesia. Trop J Nat Prod Res. 2024; 8(9):8393-8399. doi: 10.26538/tjnpr/v8i9.22
10. Shah M, Patel M, Shah M, Patel M, Prajapati M. Computational Transformation in Drug Discovery: A Comprehensive Study on Molecular Docking and Quantitative Structure Activity Relationship (QSAR). Intell Pharm. 2024; 2(5):589-595. doi: 10.1016/j.ipha.2024.03.001
11. Tamang JP. Ethnic Fermented Foods and Alcoholic Beverages of Asia. 1st ed. New Delhi: Springer India. 2016; 409p. doi: 10.1007/978-81-322-2800-4
12. Andayani SN, Lioe HN, Wijaya CH, Ogawa M. Umami Fractions Obtained from Water-soluble Extracts of Red Oncom and Black Oncom—Indonesian Fermented Soybean

and Peanut Products. J Food Sci. 2020; 85(3):657-665. doi: 10.1111/1750-3841.14942
13. Surya R, Romulo A. Antioxidant Profile of Red Oncom, an Indonesian Traditional Fermented Soyfood. Food Res. 2023; 7(4):204-210. doi: 10.26656/fr.2017.7(4).650
14. Wu F, Zhou Y, Li L, Shen X, Chen G, Wang X, Liang X, Tan M and Huang Z. Computational Approaches in Preclinical Studies on Drug Discovery and Development. Front Chem. 2020; 8(726):1-32. doi: 10.3389/fchem.2020.00726
15. OECD. Acute Oral Toxicity – Fixed Dose Procedure (chptr). OECD Guid Test Chem. OECD Publishing, Paris. 2002;1-14. doi: 10.1787/9789264070943-en
16. Ijoma IK, Okafor CE, Ajiwe VIE. Computational Studies of 5-methoxypsolaren as Potential Deoxyhemoglobin S Polymerization Inhibitor. Trop J Nat Prod Res. 2024; 8(10):8835-8841. doi: 10.26538/tjnpr/v8i10.28
17. Illian DN, Widiyana AP, Hasana AR, Maysarah H, Al Mustaniroh SS, Basyuni M. In Silico Approach: Prediction of ADMET, Molecular Docking, and QSPR of Secondary Metabolites in Mangroves. J Appl Pharm Sci. 2022; 12(11):021-029. doi: 10.7324/JAPS.2022.121103
18. Ernawati T, Artanti N, Kumiawan YD. *In Silico* and *In Vitro* Anti-cancer Activity against Breast Cancer Cell Line MCF-7 of Amide Cinnamate Derivatives. J Appl Pharm Sci. 2024; 14(3):102-107. doi: 10.7324/JAPS.2024.162177
19. Fadilah F, Andrajati R, Arsianti A, Paramita RI, Erlina L, Istiadi KA, Yanuar A. Synthesis and In Vitro Activity of Eugenyl Benzoate Derivatives as BCL-2 Inhibitor in Colorectal Cancer with QSAR and Molecular Docking Approach. Asian Pac J Cancer Prev. 2023; 24(9):2973-2981. doi: 10.31557/APJCP.2023.24.9.2973
20. Abdelli W, Hamed D. Molecular Docking and Pharmacokinetics Studies of *Syzygium aromaticum* Compounds as Potential SARS-CoV-2 Main Protease Inhibitors. Trop J Nat Prod Res. 2023; 7(11):5155-5163. doi: 10.26538/tjnpr/v7i11.18
21. Maharani DA, Adelina R, Aini AQ, Supandi. Molecular Docking and Dynamic Simulation of *Erythrina fusca* Lour Chemical Compounds Targeting VEGFR-2 Receptor for Anti-Liver Cancer Activity. J Kim Val. 2024; 10(1):106-114. doi: 10.15408/jkv.v10i1.35295
22. Zuhri UM, Purwaningsih EH, Fadilah F, Yuliana ND. Network Pharmacology Integrated Molecular Dynamics Reveals the Bioactive Compounds and Potential Targets of *Tinospora crispa* Linn. as Insulin Sensitizer. PLoS One. 2022; 17(6):1-15. doi: 10.1371/journal.pone.0251837
23. Kondža M, Brizić I, Jokić S. Flavonoids as CYP3A4 Inhibitors in Vitro. Biomedicines. 2024; 12(3):1-23. doi: 10.3390/biomedicines12030644
24. Omar AM, Aljahdali AS, Safo MK, Mohamed GA, Ibrahim SRM. Docking and Molecular Dynamic Investigations of Phenylspirodrimanes as Cannabinoid Receptor-2 Agonists. Molecules. 2023; 28(1):1-17. doi: 10.3390/molecules28010044
25. Sutherland JB, Bridges BM, Heinze TM, Adams MR, Delio PJ, Hotchkiss C, Rafii, F. Comparison of the Effects of Antimicrobial Agents from Three Different Classes on Metabolism of Isoflavonoids by Colonic Microflora Using Etest Strips. Curr Microbiol. 2012; 64(1):60-65. doi: 10.1007/s00284-011-0020-4
26. Buchmann D, Schultze N, Borchardt J, Böttcher I, Schaufler K, Guenther S. Synergistic Antimicrobial Activities of Epigallocatechin Gallate, Myricetin, Daidzein, Gallic Acid, Epicatechin, 3-Hydroxy-6-Methoxyflavone, and Genistein Combined with Antibiotics Against ESKAPE Pathogens. J Appl Microbiol. 2022; 132(2):949-963. doi: 10.1111/jam.15253.
27. Jagatap VR, Ahmad I, Sriram D, Kumari J, Adu DK, Ike BW, Ghai M, Ansari SA, Ansari IA, Wetchoua POM, Karpoormath R, Patel H. Isoflavonoid and Furanochromone Natural Products as Potential DNA Gyrase Inhibitors: Computational, Spectral, and Antimycobacterial Studies. ACS Omega. 2023; 8(18):16228-16240. doi: 10.1021/acsomega.3c00684.
28. Yang J, Xiao P, Sun J, Guo L. Anticancer Effects of Kaempferol in A375 Human Malignant Melanoma Cells are Mediated via Induction of Apoptosis, Cell Cycle Arrest, Inhibition of Cell Migration and Downregulation of m-TOR/PI3K/AKT Pathway. J BUON. 2018; 23(1):218-223. https://www.jbuon.com/archive/23-1-218.pdf
29. Kumar V and Chauhan SS. Daidzein Induces Intrinsic Pathway of Apoptosis along with ER α/β Ratio Alteration and ROS Production. Asian Pac J Cancer Prev. 2021; 22(2):603-610. doi: 10.31557/APJCP.2021.22.2.603
30. Márquez-Flores YK, Martínez-Galero E, Correa-Basurto J, Sixto-López Y, Villegas I, Rosillo MÁ, Cárdeno A, Alarcón-de-la-Lastra C. Daidzein and Equol: *Ex Vivo* and *In Silico* Approaches Targeting COX-2, iNOS, and the Canonical Inflammasome Signaling Pathway. Pharmaceuticals. 2024; 17(647):1-19. doi: 10.3390/ph17050647
31. Jia J, He R, Yao Z, Su J, Deng S, Chen K, Yu B. Daidzein Alleviates Osteoporosis by Promoting Osteogenesis and Angiogenesis Coupling. PeerJ. 2023; 11:(e16121):1-20. doi: 10.7717/peerj.16121.